Controllable excitation transmission and topological switch based on an imaginary topological channel in a non-Hermitian Su-Schrieffer-Heeger chain

Lu Qi,[1,*] Ning Han,[2] Shutian Liu,[3] Hong-Fu Wang,[4,†] and Ai-Lei He[1,‡]

[1]*School of Physical Science and Technology, Yangzhou University, Yangzhou 225002, China*
[2]*Interdisciplinary Center for Quantum Information, State Key Laboratory of Modern Optical Instrumentation, College of Information Science and Electronic Engineering, Zhejiang University, Hangzhou 310027, China*
[3]*School of Physics, Harbin Institute of Technology, Harbin, Heilongjiang 150001, China*
[4]*Department of Physics, College of Science, Yanbian University, Yanji 133002, China*

(Received 16 February 2023; revised 12 May 2023; accepted 9 June 2023; published 27 June 2023)

We show the controllable excitation transmission can be implemented based on the topologically protected edge channel in the modulated Su-Schrieffer-Heeger model with gain and loss. We find that the gain and loss open up a special edge channel with pure imaginary energy, by which the opening and closing of the topological excitation transmission between left and right edges can be controlled via tuning the amplitude of the imaginary potential. We reveal that the special edge transmission phenomenon can be comprehended using an effective lattice model only with the gain and loss at two edge sites, in which the gain or loss added on the right edge determines the opening or closing of the topological excitation transmission. Applying the concept of controllable excitation transmission into the lattice with interface, the controllable transmissions from interface site to right edge site or left edge site can be realized. If treating the interface site as the input port and treating two edge sites as output port, the present system is equivalent to a two-way topological switch. Especially, the transmission path of topological switch toward right edge or left edge can be chosen via tuning the amplitude of the imaginary potential. The controllable excitation transmission and topological switch further explore the potential applications of topological materials in quantum information processing, which may provide the enlightening suggestions for implementing the topological devices, including the topological triode and topological logical gate.

DOI: 10.1103/PhysRevA.107.062214

I. INTRODUCTION

As a basic module for large-scale quantum communication, quantum state needs to be transmitted between different nodes with large enough fidelity [1–4]. However, the existence of inherent defect or fluctuation in the channel inevitably decreases the transmission efficiency. The discovery of topological classification [5–8] in condensed matter physics opens up the new opportunity and possibility to implement robust and efficient quantum information processing [9–15]. The topological insulator, as the representative example in the topological classification of materials, exhibits completely different properties from the traditional insulator, e.g., the appearance of gapless boundary states in the gap [5–8,16–18]. Due to the topological protection originating from the global characteristic, these boundary states are immune to the backscattering caused by defect [19–25], leading the boundary state to become the reliable candidate to implement the robust topological quantum information processing ranging from robust quantum state transfer to topological distribution. For example, in the two-dimensional (2D) topological dipolar arrays, robust quantum state transfer can be implemented based on the topologically protected edge channel [13]. And the quantum communication between distant qubits has also been proposed in the 2D topological networks [14], in which the linear network of coupled bosonic degrees of freedom can be employed for the efficient exchange of quantum information over large distances. Further, the topological beam splitters with the distribution function have also been implemented based on waveguide array [15], disorder-induced bulk pumping [26], and the design of the topological domain wall [27–30].

The dimerized Su-Schrieffer-Heeger (SSH) model [31], as one of the simplest one-dimensional (1D) lattices with the nontrivial edge state, has also attracted more and more attentions on the investigations about the topological transmissions [32–39]. Different from the 2D topological system with the 1D boundary states, the 1D SSH model only has two edge sites, meaning that the SSH model usually cannot implement the robust topological transmission based on the general 1D topological edge channel. To handle it, we need to introduce an additional periodical parameter to map the second physical dimension in 2D topological systems [40–46]. Usually, the periodical parameter can be introduced via the modulated onsite energy or the hopping amplitudes [41,43,44,47,48], by which the robust topological transmission can be realized. In Ref. [33], a robust quantum state transfer scheme has been

*luqi@yzu.edu.cn
†hfwang@ybu.edu.cn
‡heailei@yzu.edu.cn

proposed based on a dimerized superconducting circuit lattice with modulation, in which the quantum state prepared at the left edge site can be transmitted to the right edge site without the influence of the local disorder. In addition to the photonic system, the acoustic edge pumping from one boundary to the opposite boundary can be implemented in the modulated acoustic lattices [49,50]. To further improve the efficiency of the topological edge transmission, the accelerated schemes of topological transmission have been proposed by using the adiabatic passage [36], designing counterdiabatic driving [38], and defining the adiabatic invariant [39]. Note that the above investigations are mainly focused on the transmission from single node to single node in the SSH lattice, which is insufficient for the construction of the large-scale topological quantum network. Thus, we have explored the schemes of topological edge transmission with two and multiple output ports [51–53]. We stress that these topological edge transmission schemes mainly focus on the Hermitian system where the non-Hermitian effects in practical open system are not considered. The non-Hermiticity usually has certain effects on the traditional quantum state transfer schemes, e.g., the unstable evolution and decreased transport efficiency induced by detrimental dissipation. However, for topological excitation transmission, whether the topological protection originating from gap can balance the detrimental effects of dissipation, is still an open issue. Especially, it is also an interesting topic whether the detrimental dissipation can be effectively utilized in designing the topological excitation transmission scheme.

Inspired by these issues, in this paper, we propose a scheme to investigate the controllable topological edge transmission of excitation from left edge site to right edge site in the modulated SSH model with the alternating gain and loss. We find that, via tuning the amplitudes of the gain and loss, the topological excitation transmission from left edge to right edge can be allowed or blocked. More specifically, when the amplitudes of gain and loss are positive, the excitation initially located at the left edge can be transmitted to the right edge successfully, while, the transmission cannot be implemented when the amplitudes of gain and loss are negative. We reveal that the controllable excitation transmission may originate from the gain or loss added on the right edge site via an effective lattice model only possessing the gain and loss at two-end sites. Based on the controllable topological excitation transmission, we find the gain and loss added into the lattice with the interface can induce the controllable excitation transmission with different transmission paths. For example, for the positive (negative) amplitudes of gain and loss, the excitation initially prepared at the interface site can be transmitted to the right (left) edge site. Thus, if regarding two topological transmissions with different direction as two output paths, the present system can be equivalent to a two-way topological switch, in which the output path can be tuned via controlling the amplitudes of gain and loss. Our finding further supplies the relevant investigations of the SSH model in topological quantum information processing, which may have potential applications in topological sensor, topological triode, and even topological logical gate.

The paper is organized as follows: In Sec. II, we demonstrate that the controllable topological excitation transmission induced via gain and loss can be implemented in the modulated SSH model. We find that the phenomenon can be interpreted via the effective SSH model with imaginary potentials added on edge sites. We also investigate the two-way topological switch based on controllable excitation transmissions and discuss the experimental feasibility. Finally, a conclusion is given in Sec. III.

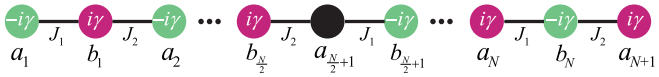

FIG. 1. The diagrammatic sketch of the SSH model with onsite imaginary potentials. The lattice contains N unit cells with the size of $L = 2N + 1$. In this lattice, each unit cell is composed by a_n and b_n sublattice sites accompanied with the intracell hopping J_1 and intercell hopping J_2. Especially, except the central site, the lattice has the alternating loss and gain before or after the central $(N + 1)$th site.

II. CONTROLLABLE EXCITATION TRANSMISSION INDUCED VIA GAIN AND LOSS IN SU-SCHRIEFFER-HEEGER MODEL

A. Model and Hamiltonian

Consider an odd-sized SSH chain with the gain and loss, as shown in Fig. 1. In this chain, the lattice contains N unit cells with the size of $L = 2N + 1$, and we take N as an even number for convenience. Note that each unit cell of the lattice is composed by a_n and b_n sublattice sites accompanied with the intracell hopping J_1 and intercell hopping J_2, respectively. Especially, except the central site, the lattice has the alternating loss and gain before or after the central $(N + 1)$th site. The lattice can be described by the following Hamiltonian:

$$\begin{aligned} H = &\sum_{n=1}^{N/2}(-i\gamma a_n^\dagger a_n + i\gamma b_n^\dagger b_n) \\ &+ \sum_{n=N/2+1}^{N}(-i\gamma b_n^\dagger b_n + i\gamma a_{n+1}^\dagger a_{n+1}) \\ &+ \sum_{n=1}^{N}(J_1 a_n^\dagger b_n + J_2 a_{n+1}^\dagger b_n + \text{H.c.}). \end{aligned} \tag{1}$$

Here γ is the strength of the gain and loss while $J_1 = J - \cos\theta$ and $J_2 = J + \cos\theta$ are the modulated amplitudes of nearest-neighbor (NN) hopping. For simplicity, we take $J = 1$ as energy unit and take $\theta \in [0,\ 2\pi]$ as the periodical parameter. In this way, the first two summations in Eq. (1) represent the pure imaginary onsite energy induced by gain and loss, and the last summation represents the modulated NN hopping between two adjacent sites. When the amplitudes of gain and loss satisfy $\gamma = 0$, the present model degenerates into a standard odd-sized SSH model. For the odd-sized SSH model, the chiral symmetry leads to the existence of the isolated zero-energy mode in the gap, in which the zero-energy mode is mainly localized at the left edge site when $J_1 < J_2$ ($\theta \in [0,\ 0.5\pi] \cup [1.5\pi,\ 2\pi]$) and is mainly localized at the right edge site when $J_1 > J_2$ ($\theta \in [0.5\pi,\ 1.5\pi]$), as shown in Figs. 2(a) and 2(b) (see the Appendix for more discussions). The zero-energy mode with the alternating localization in the

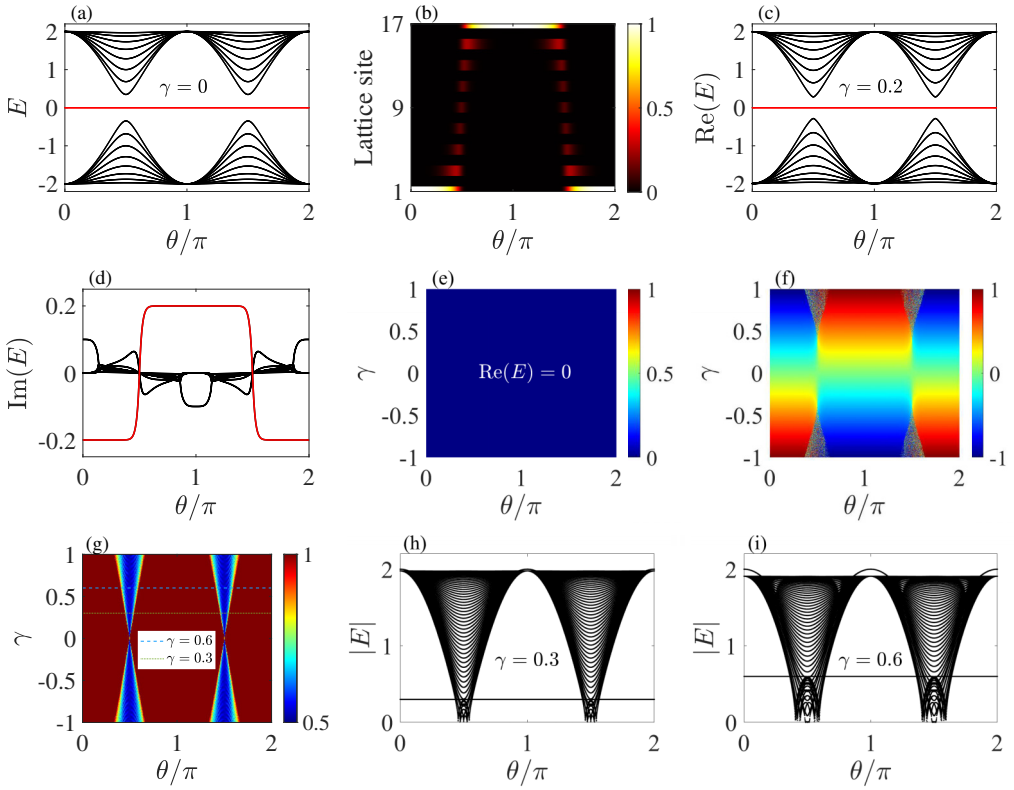

FIG. 2. Energy spectra, distributions of gap states, and phase diagram. (a) The energy spectrum of the standard SSH model when $\gamma = 0$, in which the red line represents the zero-energy mode. (b) The distribution of zero-energy mode versus the periodic parameter θ. (c) The real part of energy spectrum when $\gamma = 0.2$. (d) The corresponding imaginary part of energy spectrum when $\gamma = 0.2$. The colored lines represent the gap state with pure imaginary eigenvalue. (e) The real part of gap state versus γ and θ. (f) The imaginary part of gap state versus γ and θ. (g) Phase diagram versus $\gamma - \theta$ plane. The blue colored region represents region of gapless point while red region denotes topological insulator (TI) phase. Here parameters are set as $E_b = 0$ and $N = 200$, and we take modulus in the process of Tr' for convenience. (h), (i) The moduli of energy spectra when $\gamma = 0.3$ and $\gamma = 0.6$ for $N = 50$. $J = 1$ is chosen as the energy unit.

odd-sized SSH model is widely used to implement the topological quantum state transfer [33,36,38,39,51], which gives the typical application of topological insulator in quantum information processing.

However, when the gain and loss satisfy $\gamma \neq 0$, the introduction of the pure imaginary potentials may lead to the appearance of the complex energy, which further influences the topological transmission assisted by the topological edge channel. For example, when $\gamma = 0.2$, the real and imaginary parts of the energy spectrum are shown in Figs. 2(c) and 2(d). Although the real part of the energy spectrum is similar with the case when $\gamma = 0$, the appearance of the imaginary part implies that the system changes from the Hermitian case to non-Hermitian case. Note that the real part of the energy spectrum also has a zero-energy mode [red line in Fig. 2(c)] but it corresponds to a nonzero imaginary part [red line in Fig. 2(d)]. Thus, if we use the present topological edge channel to implement the topological transmission now, the edge channel with pure imaginary eigenvalue may have effects on the dynamical stability of evolution. The zero-energy mode in the real part of the energy spectrum and its corresponding imaginary part versus the parameters θ and γ are plotted in Figs. 2(e) and 2(f). The results reveal that the gain and loss cannot influence the zero-energy mode in the real part of the energy spectrum. However, for the case of $\gamma > 0$ ($\gamma < 0$), the corresponding imaginary part of the zero-energy mode is equal to $-\gamma$ (γ) within $\theta \in [0,\ 0.5\pi] \cup [1.5\pi,\ 2\pi]$ while is equal to γ ($-\gamma$) when $\theta \in [0.5\pi,\ 1.5\pi]$ (see the Appendix for more discussions). Especially, we find that the large enough gain and loss, e.g., $|\gamma| > 0.5$, the non-Hermiticity makes the Hamiltonian cannot be diagonalized precisely around the closing point of gap ($\theta = 0.5\pi$ and 1.5π).

The closing point of the gap can be further captured via the phase diagram defined by non-Hermitian winding number in real space [54,55], i.e., $W = \frac{1}{L'}\mathrm{Tr}'(Q^\dagger[Q, X])$. Here, X denotes the position operator, $L' = L - 2l$ is the effective length of bulk after excluding a certain edge length $l = 0.4N$, and Tr' represents the trace taken only over effective bulk length. Furthermore, the operator $Q = UV^\dagger$ is defined via a singular value decomposition $H - E_b I = U\Lambda V^\dagger$ (Λ is the diagonal matrix) after choosing a base energy E_b. The phase diagram is shown in Fig. 2(g) in which the red region represents the topologically nontrivial phase while the blue colored region corresponds to the region for closing point of gap with ill-defined winding number. Obviously, the region in which the Hamiltonian cannot be diagonalized precisely in Fig. 2(f) agrees well with the region for the closing point of the gap. To further verify the phase diagram, the moduli of energy spectra when $\gamma = 0.3$ and 0.6 are plotted in Figs. 2(h) and 2(i). The energy spectra clearly exhibit corresponding

windows of gapless points which are extended with the increasing of parameter γ. Different from the Hermitian version of topological quantum state transfer in the standard SSH model, the window of gapless points originating from the pure imaginary eigenenergy of gap state may lead to the evolution of the quantum state becoming instable and entering into the bulk states. Thus, the effects of the edge channel with pure imaginary eigenvalue on topological quantum state transfer should be further estimated.

B. Controllable topological excitation transmission

To further explore the effects of the edge channel with pure imaginary eigenvalue on the topological transmission, we first recall the adiabatic evolution of the edge channel. As shown in Fig. 2(b), for the given initial left edge state $|L\rangle = |\psi_{a_1}, \psi_{b_1}, \ldots, \psi_{a_N}, \psi_{b_N}, \psi_{a_{N+1}}\rangle = |1, 0, \ldots, 0, 0, 0\rangle$, it will be evolved under the domination of the Schrödinger equation $i\frac{\partial}{\partial t}|L\rangle = H(\theta_t)|L\rangle$, if we rewrite the periodical parameter θ as the form of multiplication between varying rate Ω and time t, i.e., $\theta = \Omega t$. Ideally, when the varying rate Ω is small enough, the initial left edge state $|L\rangle$ will evolve along the zero-energy mode and finally reaches the right edge state $|R\rangle = |0, 0, \ldots, 0, 0, 1\rangle$ at the final time $t_{\text{end}} = \pi/\Omega$. In this way, the reliability of the edge channel can be evaluated quantitatively via the fidelity F between the practical evolved final state $|\Psi_f\rangle$ and the ideal final state $|R\rangle$ with $F = |\langle R|\Psi_f\rangle|$. Thus, when fidelity satisfies $F \sim 1$, the evolution between the left edge state $|L\rangle$ and right edge state $|R\rangle$ can be implemented successfully, meaning that the excitation initially prepared at the left edge can be transmitted to the right edge (see more discussions in the Appendix).

The fidelity F versus the varying rate Ω and imaginary potential amplitude γ, when the system has the gain and loss, is plotted in Fig. 3(a). Here, the blank region around $\log_{10}(\Omega) = -3$ and $|\gamma| > 0.5$ in Fig. 3(a) represents the invalid region for normalization of the evolved final state induced by the strong non-Hermiticity. Furthermore, the fidelity exhibits a special region [yellow colored region in Fig. 3(a)] with $F \sim 1$ when $\gamma > 0$. Thus, we can control the excitation transmission from the left edge to right edge via tuning the varying rate Ω and imaginary potential amplitude γ in this region. Actually, the method of tuning the varying rate Ω is equivalent to control the adiabatic evolution condition, which has been revealed in many previous works [36,38,39,51]. However, the later method on tuning the imaginary potential amplitude γ is what we mainly focused in this work. The fidelity F versus γ for the given Ω is shown in Fig. 3(b). Obviously, the fidelity keeps $F = 0$ when $\gamma < 0$ and changes as $F = 1$ when $\gamma > 0$, meaning that the excitation transmission between two edges can only be implemented within $\gamma > 0$. For example, when $\Omega = 0.02$ and $\gamma = -0.2$, the state transfer between $|L\rangle$ and $|R\rangle$ cannot be implemented successfully, as shown in Fig. 3(c). On the contrary, when $\Omega = 0.02$ and $\gamma = 0.2$, the excitation initially at the left edge can be transmitted to the right edge, as shown in Fig. 3(d). In this way, we can control the excitation transmission between two edges via tuning the imaginary potential amplitude γ, e.g., opening the transmission when $\gamma > 0$ and closing the transmission when $\gamma < 0$.

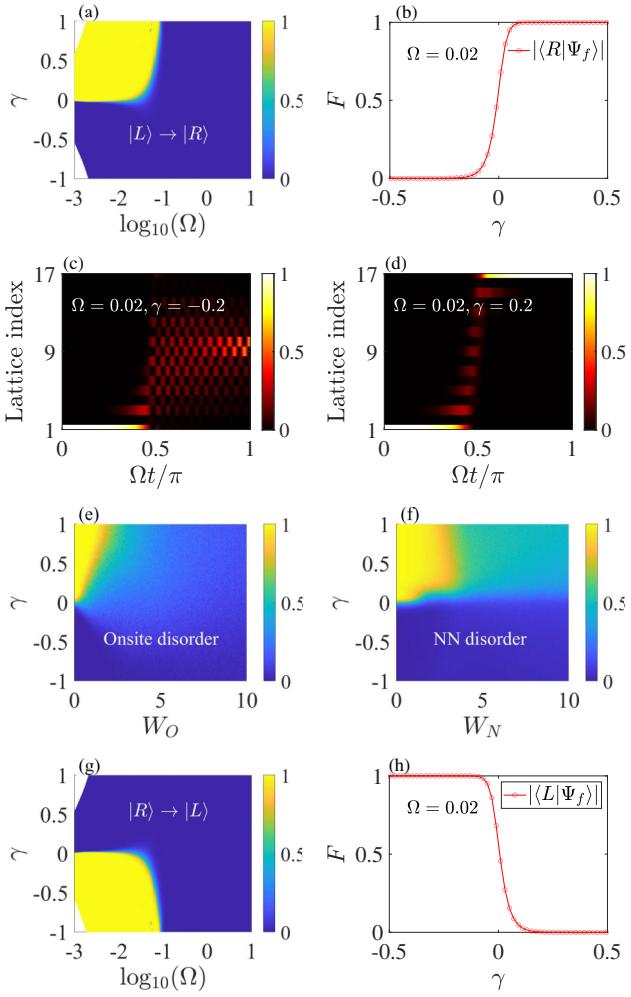

FIG. 3. Fidelity and the process of topological excitation transmission. (a) Fidelity F versus the varying rate Ω and imaginary potential strength γ. (b) Fidelity F versus the imaginary potential strength γ when $\Omega = 0.02$. (c) The process of topological excitation transmission when $\Omega = 0.02$ and $\gamma = -0.2$. (d) The process of topological excitation transmission when $\Omega = 0.02$ and $\gamma = 0.2$. (e) Fidelity F versus the onsite disorder amplitude W_O and imaginary potential strength γ when $\Omega = 0.02$. (f) Fidelity F versus the disorder amplitude in NN hopping W_N and imaginary potential strength γ when $\Omega = 0.02$. (g) Fidelity F for excitation transmission from the right edge to left edge versus the varying rate Ω and imaginary potential strength γ. (h) Fidelity F for excitation transmission from the right edge to left edge versus the imaginary potential strength γ when $\Omega = 0.02$. $J = 1$ is chosen as the energy unit.

Benefiting from the protection of gap, the present controllable excitation transmission between two edges is also immune to the mild disorders, e.g., onsite disorder $H_O = \sum_{n=1}^{N/2} W_O(-i\delta_{a,n}a_n^\dagger a_n + i\delta_{b,n}b_n^\dagger b_n) + \sum_{n=N/2+1}^{N} W_O(-i\delta_{b,n}b_n^\dagger b_n + i\delta_{a,n+1}a_{n+1}^\dagger a_{n+1})$ or disorder in NN hopping $H_{\text{NN}} = \sum_n W_N[(\delta_{1,n}a_n^\dagger b_n + \delta_{2,n}a_{n+1}^\dagger b_n) + \text{H.c.}]$. Here, W_O (W_N) is the disorder amplitude added into imaginary onsite potential (NN hopping), $\delta_{j,n}$ with $j = a, b, 1, 2$ denotes the uniform random quantity within the range of $[-0.5, 0.5]$. The fidelities for the excitation transmission from the left edge to right edge versus disorder amplitudes and non-Hermitian

parameter γ are plotted in Figs. 3(e) and 3(f). Here, we numerically calculate the average fidelities after taking 100 times of disorder samples. The results reveal that the excitation transmission from left edge to right edge can be implemented within a certain range of disorder amplitudes, implying the robustness of the controllable excitation transmission. Especially, for the order of magnitude, the present topological excitation transmission can resist larger disorder added in NN hopping compared with the onsite disorder, while the evolution process is much more robust to the onsite disorder (see more discussions in the Appendix).

Aside from the controllable excitation transmission from left edge to right edge, we can implement the reverse excitation transmission via exchanging the sign of parameter γ. For example, when parameter γ satisfies $\gamma < 0$, the excitation transmission from the right edge to left edge can be implemented via varying periodic parameter θ within $[\pi, 2\pi]$ and choosing appropriate varying rate Ω. The fidelity for the excitation transmission from right edge to left edge, i.e., $F = \langle L|\Psi_f\rangle$, versus parameters Ω and γ is plotted in Fig. 3(g), in which the window of $F \sim 1$ indicates the feasible excitation transmission from right edge to left edge via setting $\gamma < 0$. Similarly, the excitation transmission from right edge to left edge can be opened or closed controllably by setting $\gamma < 0$ or $\gamma > 0$, as shown in Fig. 3(h).

C. Effective model for controllable topological excitation transmission

To explain the reason of the above controllable topological excitation transmission, we now introduce a simple effective model. We stress that the above topological excitation transmission is essentially based on the gap state of system, which can be determined via its eigenenergy (see more discussions in the Appendix). Note that, for the large size of lattice chain (e.g., lattice chain under thermodynamic limit), edge sites can be regarded as perturbation compared with bulk, meaning the onsite energy added on edge (bulk) sites almost has no effects on the bulk (edge) states energy. In other words, onsite energy added on edge sites mainly determines the eigenenergy of gap states. This can also be comprehended via the fact that edge states are mainly localized around edge sites, leading edge states are much more sensitive to the onsite energy added on edge sites. As a result, although the gain and loss are added on multiple sites, only the gain and loss added on both edge sites have the greatest effects on the gap state. Thus, the controllable excitation transmission can be revealed via an effective lattice model only possessing the gain and loss at two-end sites, namely,

$$H' = (-i\gamma a_1^\dagger a_1 + i\gamma a_{2N+1}^\dagger a_{2N+1}) + \sum_{n=1}^{N}(J_1 a_n^\dagger b_n + J_2 a_{n+1}^\dagger b_n + \text{H.c.}). \quad (2)$$

To verify above deduction, we plot the energy spectrum of the effective model when $\gamma = 0.2$, as shown in Figs. 4(a) and 4(b). Compared with the results in Figs. 2(c) and 2(d), the effective model exhibits the similar energy spectrum, revealing that the effective model may have the similar controllable excitation transmission. The fidelity F' between the right edge state $|R\rangle$ and evolved final state $|\Psi_f'\rangle$ dominated by Hamiltonian H' versus γ and Ω is plotted in Fig. 4(c). The fidelity F' exhibits the consistent behavior compared with the original lattice model. For example, as illustrated in Figs. 4(d)–4(f), the excitation transmission in the effective model also can be implemented when $\gamma > 0$ and becomes invalid when $\gamma < 0$. These results together prove that the insightful physics of the original model can be effectively captured by the effective model.

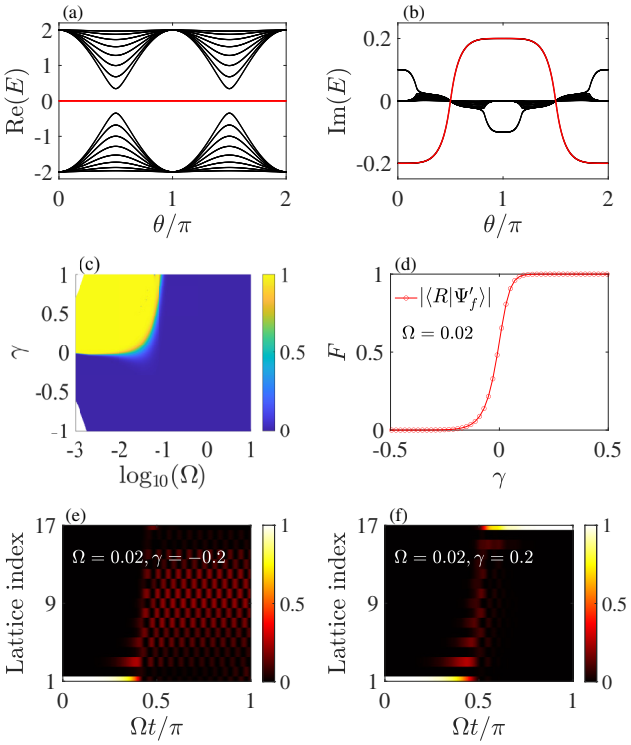

FIG. 4. Energy spectra, fidelity, and topological excitation transmission for the effective model. (a) The real part of energy spectrum for the effective model when $\gamma = 0.2$. (b) The imaginary part of energy spectrum for the effective model when $\gamma = 0.2$. (c) Fidelity F' versus the varying rate Ω and imaginary potential strength γ in the effective model. (d) Fidelity F' versus the imaginary potential strength γ when $\Omega = 0.02$. (e), (f) When $\Omega = 0.02$, the processes of topological excitation transmission in the effective model for $\gamma = -0.2$ and 0.2. $J = 1$ is chosen as the energy unit.

In this way, for the initial state $|L\rangle = |\psi_{a_1}, \psi_{b_1}, \ldots, \psi_{a_N}, \psi_{b_N}, \psi_{a_{N+1}}\rangle$, its probability amplitudes, in the process of evolution under the domination of effective model, satisfy

$$\begin{aligned}
\dot{\psi}_{a_1} &= -\gamma\psi_{a_1} - iJ_1\psi_{b_1}, \\
\dot{\psi}_{b_n} &= -iJ_1\psi_{a_n} - iJ_2\psi_{a_{n+1}} \ (n = 1, \ldots, N), \\
\dot{\psi}_{a_n} &= -iJ_2\psi_{b_{n-1}} - iJ_1\psi_{b_n} \ (n = 2, \ldots, N), \\
\dot{\psi}_{a_{N+1}} &= \gamma\psi_{a_{N+1}} - iJ_2\psi_{b_N}.
\end{aligned} \quad (3)$$

When $\gamma \sim 0$, the system can be assumed to still keep Hermitian, and the evolution of the initial state still goes along the zero-energy mode only possessing the distributions on odd sites. Thus, probability amplitudes at two-end sites can be

approximately written as $\psi_{a_1}(t) = e^{-\gamma t}$ and $\psi_{a_{N+1}}(t) = e^{\gamma t}$. Obviously, the probability amplitude $\psi_{a_{N+1}}$ at last site is amplified when $\gamma > 0$ and finally is mainly localized at right edge site after normalization. However, when $\gamma < 0$, the amplified probability amplitude ψ_{a_1} is transmitted to $\psi_{a_{N+1}}$ and finally decays to zero quickly, implying that the transmission from left to right cannot be implemented for $\gamma < 0$. Moreover, when the imaginary potential amplitude γ is large enough, the large enough $\psi_{a_1} \sim \infty$ or $\psi_{a_{N+1}} \sim \infty$ induced by rapid exponential growth also leads to the invalidity of the normalization.

D. Topological beam splitter and two-way topological switch

The controllable topological excitation transmission induced via gain and loss in the SSH lattice may have potential applications in the field of topological quantum information processing. For example, if applying the method of controllable topological excitation transmission into the topological beam splitter scheme in Ref. [52], the topological beam splitter with controllable two-way transmissions can be implemented. More specifically, when the system has gain and loss, the topological beam splitter in Ref. [52] now becomes

$$\begin{aligned} H_{\mathrm{TBS}} = & \sum_{n}[-V(a_n^\dagger a_n - b_n^\dagger b_n)] + \sum_{n=1}^{N/2}[-i\gamma(a_n^\dagger a_n - b_n^\dagger b_n) \\ & + (J_2 a_n^\dagger b_n + J_1 a_{n+1}^\dagger b_n + \mathrm{H.c.})] \\ & + \sum_{n=N/2+1}^{N}[-i\gamma(b_n^\dagger b_n - a_{n+1}^\dagger a_{n+1}) \\ & + (J_1 a_n^\dagger b_n + J_2 a_{n+1}^\dagger b_n + \mathrm{H.c.})]. \end{aligned} \tag{4}$$

Here $V = \sin\theta$ is the alternating onsite energy, γ represents the amplitude of imaginary potentials, and $J_j = 1 + (-1)^j \cos\theta$ $(j = 1, 2)$ still is the modulated NN hopping. When $\gamma = 0$, the present model just corresponds to the topological beam splitter in Ref. [52], in which the initial excitation at the interface site can be transmitted toward two ends and finally appears at two ends with the equal half-probability, as shown in Fig. 5(a). The transmission of the topological beam splitter when $\gamma \neq 0$ is plotted in Figs. 5(b) and 5(c). Obviously, when $\gamma = 0.2$ ($\gamma = -0.2$) the excitation initially prepared at the interface site now can only transmit toward the right (left) edge site, which determines the position of output port for topological beam splitter. This controllable topological beam splitter can choose one of two different transmission paths via tuning the imaginary potential amplitude γ, which greatly expands the application scope of the topological beam splitter.

For the given initial interface state $|I\rangle = |0, 0, \ldots, 0, 1, 0, \ldots, 0, 0\rangle$, after the evolution of the Hamiltonian H_{TBS}, the more detailed behavior of the controllable topological beam splitter can be further captured via the fidelity $F_1 = |\langle L|\Psi_f^{\mathrm{TBS}}\rangle|$ ($F_2 = |\langle R|\Psi_f^{\mathrm{TBS}}\rangle|$) between ideal final state $|L\rangle$ ($|R\rangle$) and the evolved final state $|\Psi_f^{\mathrm{TBS}}\rangle$. Estimate the effects of the imaginary potential on the fidelities F_1 and F_2, respectively. The joint fidelity $F_{\mathrm{joint}} = F_1 - F_2$ versus the varying rate Ω and imaginary potential amplitude γ is shown in Fig. 5(d). In this way, the joint fidelity $F_{\mathrm{joint}} = 1$ (red region) corresponds to $F_1 = 1$ while $F_{\mathrm{joint}} = -1$ (blue region) represents $F_2 = 1$. Thus, when the parameters are within the red (blue) region with $F_1 = 1$ ($F_2 = 1$), the topological beam splitter can only transmit the excitation at interface site to the left (right) edge site, meaning that we indeed can control the transmission paths of the topological beam splitter via choosing the appropriate γ. The detailed varying of F_1 and F_2 when $\Omega = 0.01$ is illustrated in the inset of Fig. 5(d). Obviously, for the given Ω, the fidelity F_1 keeps $F_1 = 1$ when $\gamma < 0$ and suddenly change to $F_1 = 0$ after $\gamma = 0$, while the fidelity F_2 keeps $F_2 = 0$ when $\gamma < 0$ and suddenly jump to $F_2 = 1$ after $\gamma = 0$, implying that the transmission paths of the topological beam splitter toward left and right edges are switched at the point of $\gamma = 0$. Thus, if we regard the above switched process as a switch, the present controllable beam splitter is naturally equivalent to a two-way topological switch controlled via γ, e.g., opening the right output path via $\gamma > 0$ or opening the left output path via $\gamma < 0$ [see Fig. 5(e)]. The two-way topological switch can further supply the application of topological materials in

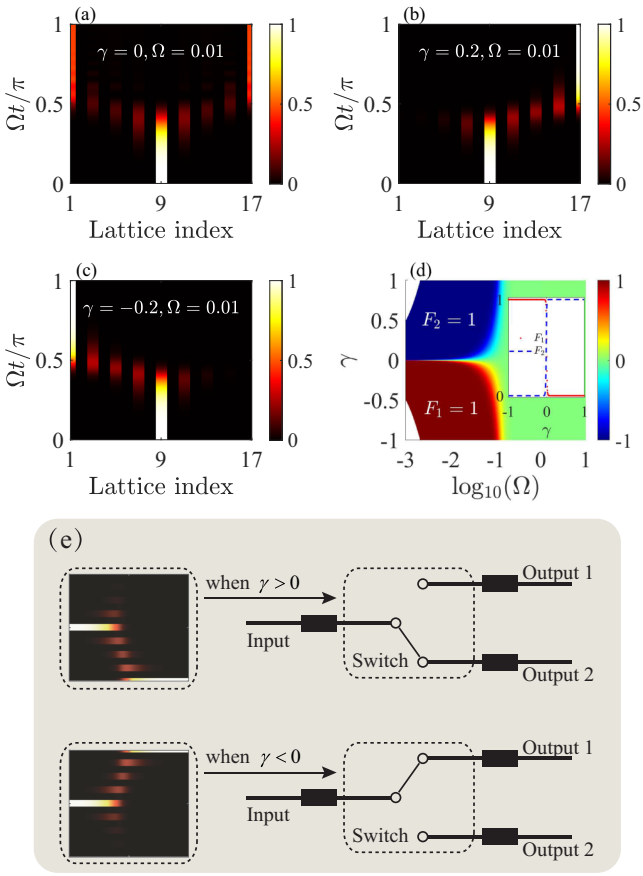

FIG. 5. Topological beam splitter and two-way topological switch. (a) The transmission of topological beam splitter when $\gamma = 0$. (b) The transmission of topological beam splitter from interface site to right edge site when $\gamma = 0.2$ and $\Omega = 0.01$. (c) The transmission of topological beam splitter from interface site to left edge site when $\gamma = -0.2$ and $\Omega = 0.01$. (d) Joint fidelity versus the varying rate Ω and imaginary potential strength γ. (e) Schematic diagram of topological two-way switch. If regarding the interface site as the input port and regarding two edge sites as two output ports, the transmission path can be controllably selected via tuning the strength of imaginary potential.

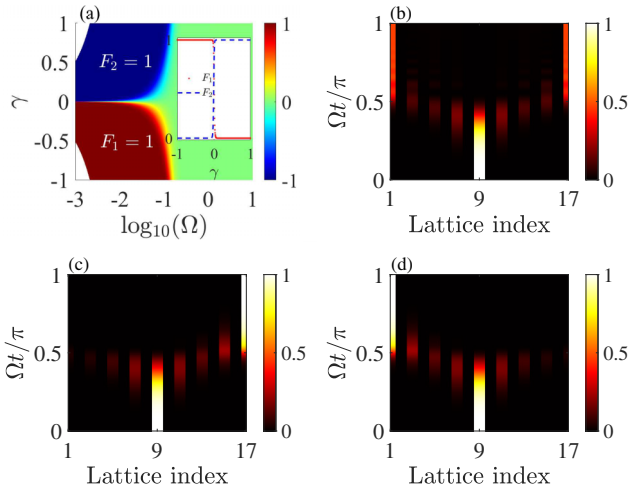

FIG. 6. Fidelity and the process of topological excitation transmission for H'_{TBS}. (a) Joint fidelity versus the varying rate Ω and imaginary potential strength γ. (b) The process of topological excitation transmission when $\Omega = 0.01$ and $\gamma = 0$. (c) The process of topological excitation transmission when $\Omega = 0.01$ and $\gamma = 0.2$. (d) The process of topological excitation transmission when $\Omega = 0.01$ and $\gamma = -0.2$. $J = 1$ is chosen as the energy unit.

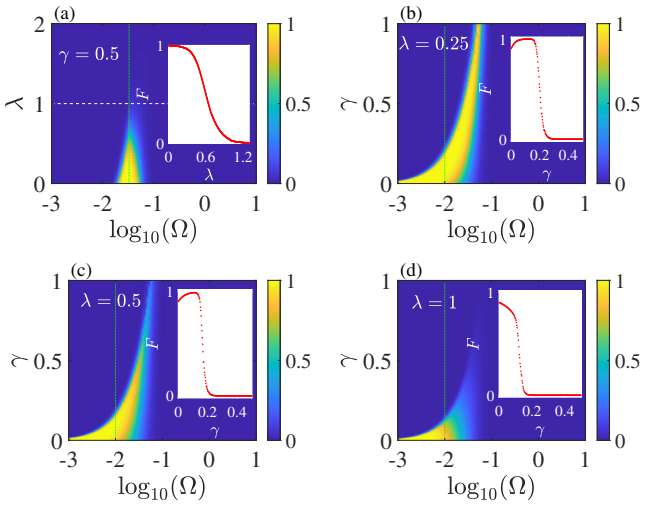

FIG. 7. Fidelity of topological excitation transmission for model with effective gain. (a) Fidelity F versus the varying rate Ω and ratio parameter λ when $\gamma = 0.5$. (b) Fidelity F versus the varying rate Ω and parameter γ when $\lambda = 0.25$. (c) Fidelity F versus the varying rate Ω and parameter γ when $\lambda = 0.5$. (d) Fidelity F versus the varying rate Ω and parameter γ when $\lambda = 1$. In all cases, the insets show the change of fidelities along the green lines. $J = 1$ is chosen as the energy unit.

quantum optical devices, which may have enlightenment for the design of topological triode, topological sensor, and even topological logical gate.

Note that the above two-way topological switch can also be comprehended by the effective model only having gain and loss at two-end sites, namely,

$$\begin{aligned} H'_{\mathrm{TBS}} = & -i\gamma[(a_1^\dagger a_1 - a_{2N+1}^\dagger a_{2N+1})] \\ & + \sum_n [-V(a_n^\dagger a_n - b_n^\dagger b_n)] \\ & + \sum_{n=1}^{N/2} (J_2 a_n^\dagger b_n + J_1 a_{n+1}^\dagger b_n + \mathrm{H.c.}) \\ & + \sum_{n=N/2+1}^{N} (J_1 a_n^\dagger b_n + J_2 a_{n+1}^\dagger b_n + \mathrm{H.c.}). \end{aligned} \tag{5}$$

The joint fidelity $F_{\mathrm{joint}} = F_1 - F_2$ under the domination of Hamiltonian H'_{TBS} is shown in Fig. 6(a). Here, $F_1 = |\langle L|\Psi_f^{\mathrm{TBS}'}\rangle|$ ($F_2 = |\langle R|\Psi_f^{\mathrm{TBS}'}\rangle|$) represent the fidelity between the ideal final state $|L\rangle$ ($|R\rangle$) and evolved final state $|\Psi_f^{\mathrm{TBS}'}\rangle$. Obviously, the pattern of fidelities agrees well with the case shown in Fig. 5(d), implying the validity of the effective model. Specifically, the effective model is degenerated as the Hermitian TBS when $\gamma = 0$, as shown in Fig. 6(b). However, when $\gamma \neq 0$, the effective model is also equivalent to a controllable two-way topological switch, as revealed in Figs. 6(c) and 6(d).

E. Experiment and discussion

Before conclusion, we give a brief discussion on the experimental feasibility. Waveguide array composed by a series of single waveguide is widely used to simulate and map topological issues [56–61]. The modulated onsite energy or the modulated coupling between two adjacent waveguides can be easily implemented via tuning the internal refractive index of waveguide [57] or changing the space between two waveguides [61]. Thus, the topological model with the modulated NN hopping and onsite energy can be easily constructed based on the waveguide array. Besides, the waveguide with the gain and loss has also been investigated widely and deeply [62–66], leading the mapping of the topological model with gain and loss to be feasible. Note that the gain term can usually be implemented via doping gain media or be effectively mapped by the smaller loss. For the effective gain mapped by smaller loss, we can describe it via an effective model, i.e.,

$$\begin{aligned} H_e = & \sum_{n=1}^{N/2} (-i\gamma_1 a_n^\dagger a_n - i\gamma_2 b_n^\dagger b_n) \\ & + \sum_{n=N/2+1}^{N} (-i\gamma_1 b_n^\dagger b_n - i\gamma_2 a_{n+1}^\dagger a_{n+1}) \\ & + \sum_{n=1}^{N} (J_1 a_n^\dagger b_n + J_2 a_{n+1}^\dagger b_n + \mathrm{H.c.}). \end{aligned} \tag{6}$$

Here, $\gamma_2 = \lambda\gamma_1 = \lambda\gamma > 0$ represents the overall loss added into the system. Thus, the terms of $-i\gamma_2 b_n^\dagger b_n$ and $-i\gamma_2 a_{n+1}^\dagger a_{n+1}$ are equivalent to the effective gain terms when $\lambda < 1$ due to the fact of $\gamma_2 < \gamma_1$. Obviously, if we vary the parameter λ from $\lambda < 1$ to $\lambda > 1$, the terms about γ_2 correspond to change from effective gain to loss, which is equivalent to the case that γ in Eq. (1) changes from $\gamma > 0$ to $\gamma < 0$. The fidelity versus varying speed Ω and parameter λ for the excitation transmission from left edge to right edge under the domination of Eq. (6) is plotted in Fig. 7(a). The white line in Fig. 7(a) denotes the case of $\gamma_1 = \gamma_2$ which corresponds to a

lattice chain with the uniform dissipations. Obviously, if we vary the parameter λ from $\lambda < 1$ to $\lambda > 1$, e.g., the green line in Fig. 7(a), the controllable excitation transmission from left edge to right edge can be implemented [see inset in Fig. 7(a)]. For example, opening the topological excitation transmission from left to right via choosing $\lambda < 0.6$, or closing the topological excitation transmission via choosing $\lambda > 0.6$.

Note that, compared with the theoretical analysis, the real transition point of the excitation transmission is around $\lambda \approx 0.6$ rather than $\lambda = 1$. The reason can be comprehended via tightening restriction of effective gain from $\gamma_1 > \gamma_2$ to $\gamma_1 \gg \gamma_2$, e.g., $\gamma_1 > 2\gamma_2$ or $\lambda < 0.5$ (at a rough estimate). More specifically, only the difference between loss rate γ_1 and loss rate γ_2 is large enough, the smaller loss rate γ_2 can be regarded as the effective gain. For example, when $\lambda = 0.25$, we can always find an appropriate varying rate Ω to implement the excitation transmission via controlling parameter γ within certain range, as shown in Fig. 7(b). When $\lambda = 0.5$, although we can implement the excitation transmission, the optional range of the parameters γ and Ω becomes small, as revealed in Fig. 7(c). Especially, when $\gamma = 1$, the system just becomes a lattice chain with overall uniform dissipations, meaning the increasing dissipations will destroy the evolution of the initial state, as shown in Fig. 7(d). Thus, we can use the method of effective gain to implement the controllable excitation transmission in experiment.

III. CONCLUSIONS

In conclusion, we have proposed a scheme to investigate the controllable topological excitation transmission in a modulated SSH model with the alternating gain and loss. We find that the topological excitation transmission from left edge to right edge can be controlled by tuning the strength of the gain and loss, e.g., allowing the topological excitation transmission when $\gamma > 0$ and prohibiting the transmission when $\gamma < 0$. The controllable excitation transmission induced via gain and loss can be further comprehended via an effective lattice model with the pure imaginary potentials only added on two edge sites, in which the positive or negative edge potential added on the right edge fundamentally determines the opening and closing for the excitation transmission. Extending the controllable excitation transmission scheme to the lattice with interface, the excitation initially prepared at the interface site can be transmitted to right edge or left edge in a controllable way. This topological excitation transmission with the tunable direction can be equivalent to a two-way topological switch, which greatly enriches the relevant investigations on the topological quantum optical devices.

ACKNOWLEDGMENT

This work was supported by the National Natural Science Foundation of China under Grants No. 12204404 and No. 12074330.

APPENDIX

1. Topological edge channel when $\gamma = 0$ and $\gamma \neq 0$

The standard odd-sized SSH model [when $\gamma = 0$ for Eq. (1)] has chiral symmetry, i.e., $CHC^{-1} = -H$ with $C = \mathrm{diag}(1, -1, \ldots, 1, -1, 1)$ being the chiral operator in real space. The chiral symmetry ensures that the eigenvalues appear in pairs, namely, $E_+ = -E_-$. Hence, there exists an isolated eigenvalue needing to be paired with itself, which leads to the existence of zero-energy eigenvalue $E_{0,+} = -E_{0,-} = 0$. The eigenstate of zero-energy eigenvalue naturally corresponds to the gap state due to the fact that zero-energy eigenvalue is located between up and bottom energy bands. If we assume the zero-energy eigenstate as $|\Psi_g\rangle = |\psi_{a_1}, \psi_{b_1}, \ldots, \psi_{a_N}, \psi_{b_N}, \psi_{a_{N+1}}\rangle$, according to the eigenenergy equation $H|\Psi_g\rangle = E_0|\Psi_g\rangle$, the amplitudes of zero-energy eigenstate satisfy

$$\begin{aligned} J_1\psi_{b_1} &= 0, \\ J_1\psi_{a_n} + J_2\psi_{a_{n+1}} &= 0 \;\; n \in [1, N], \\ J_2\psi_{b_n} + J_1\psi_{b_{n+1}} &= 0 \;\; n \in [1, N-1], \\ J_2\psi_{b_N} &= 0. \end{aligned} \tag{A1}$$

The boundary condition determines $\psi_{b,n} = 0$ with $n = (1, 2, \ldots, N)$, meaning the zero-energy gap state dose not occupy the even sites. Thus, we have $|\Psi_g\rangle = |1, 0, \eta, 0, \ldots, \eta^{N-1}, 0, \eta^N\rangle$ after setting $\psi_{a,1} = 1$ and $\eta = -J_1/J_2$. Obviously, the zero-energy gap state is mainly localized at left (right) edge when $J_1 < J_2$ ($J_1 > J_2$), providing the foundation of implementing topological excitation transmission via varying J_1 and J_2.

When parameter $\gamma \neq 0$, the eigenenergy of the gap state will be changed due to the fact that onsite energy usually can move the energy level. For simplicity, we can assume the eigenenergy of left and right edge states as $E_{g,L}$ and $E_{g,R}$ since two edges are added different onsite potentials $-i\gamma a_1^\dagger a_1$ and $i\gamma a_{N+1}^\dagger a_{N+1}$. Thus, the eigenenergy equation for left edge state now becomes $H|\Psi_{g,L}\rangle = E_{g,L}|\Psi_{g,L}\rangle$, i.e.,

$$\begin{aligned} J_1\psi_{a_n} \pm i\gamma\psi_{b_n} + J_2\psi_{a_{n+1}} &= E_{g,L}\psi_{b_n}, \\ J_2\psi_{b_n} \mp i\gamma\psi_{a_{n+1}} + J_1\psi_{b_{n+1}} &= E_{g,L}\psi_{a_{n+1}}. \end{aligned} \tag{A2}$$

Here, symbol $\pm$ ($\mp$) in the upper (lower) equation denotes $n \in [1, \frac{N}{2}]$ ($n \in [1, \frac{N}{2} - 1]$) and $n \in [\frac{N}{2} + 1, N]$ ($n \in [\frac{N}{2} + 1, N - 1]$), respectively. Aside from the bulk equations, we can also obtain three boundary equations

$$\begin{aligned} -i\gamma\psi_{a_1} + J_1\psi_{b_1} &= E_{g,L}\psi_{a_1}, \\ J_2\psi_{b_{\frac{N}{2}}} + J_1\psi_{b_{\frac{N}{2}+1}} &= E_{g,L}\psi_{a_{\frac{N}{2}+1}}, \\ J_2\psi_{b_N} + i\gamma\psi_{a_{N+1}} &= E_{g,L}\psi_{a_{N+1}}. \end{aligned} \tag{A3}$$

To solve the above equations, we need to obtain the eigenenergy of the left edge state. Note that, for the large size of lattice chain (e.g., semi-infinite lattice chain or lattice chain under thermodynamic limit), edge sites can be regarded as perturbation compared with bulk, meaning the onsite energy added on edge (bulk) sites almost has no effects on the bulk (edge) states energy. In other words, onsite energy added on edge sites mainly determines the eigenenergy of edge states. Thus, we can take the assumption of $E_{g,L} = -i\gamma$ for eigenenergy of left edge state due to the existence of $-i\gamma a_1^\dagger a_1$. In this way, the non-Hermitian terms in the bulk and boundary equations [see Eqs. (A2) and (A3)] can be eliminated via the assumption of $E_{g,L} = -i\gamma$, which reveals that the edge state

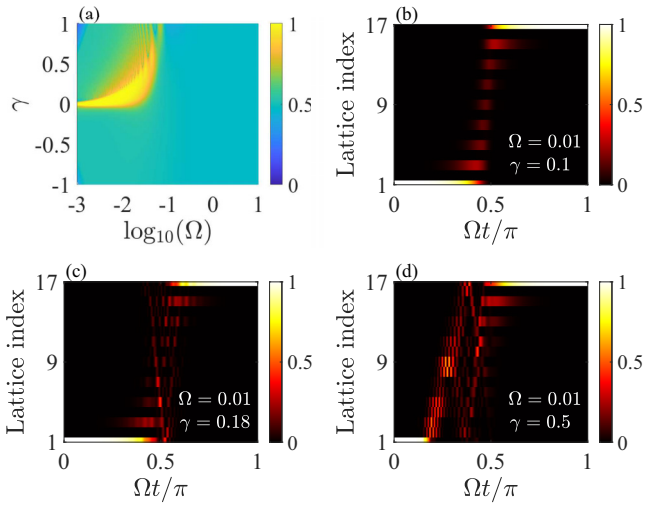

FIG. 8. Average fidelity $\bar{F}$ and process of excitation transmission. (a) Fidelity $\bar{F}$ versus the varying rate Ω and imaginary potential strength γ. (b) The process of excitation transmission when $\Omega = 0.01$ and $\gamma = 0.1$. (c) The process of excitation transmission when $\Omega = 0.01$ and $\gamma = 0.18$. (d) The process of excitation transmission when $\Omega = 0.01$ and $\gamma = 0.5$. $J = 1$ is chosen as the energy unit.

is insensitive to the imaginary potentials added on bulk sites. After that, we have

$$\begin{aligned}
\psi_{b_n} &= 0 \;\; n \in \left[1, \frac{N}{2}\right], \\
\psi_{a_{n+1}} &= -J_1/J_2 \psi_{a_n} \;\; n \in \left[1, \frac{N}{2}\right], \\
\psi_{b_{\frac{N}{2}+1}} &= -i\gamma/J_1 \psi_{a_{\frac{N}{2}+1}}, \\
\psi_{a_{n+1}} &= -J_1/J_2 \psi_{a_n} \;\; n \in \left[\frac{N}{2}+1, N\right], \\
J_2\psi_{b_n} + J_1\psi_{b_{n+1}} &= -2i\gamma\psi_{a_{n+1}} \;\; n \in \left[\frac{N}{2}+1, N-1\right], \\
\psi_{b_N} &= -2i\gamma/J_2 \psi_{a_{N+1}}. \qquad \text{(A4)}
\end{aligned}$$

Obviously, the left edge state satisfies $\psi_{a_{n+1}} = -J_1/J_2\psi_{a_n}$ for $n \in [1, N]$, i.e., $\psi_{a_{n+1}} = (-J_1/J_2)^{n-1}\psi_{a_1}$. Thus, if we set $\psi_{a_1} = 1$ and $|-J_1/J_2| < 1$, the amplitude ψ_{a_n} of left edge state at a-type site will be decreased exponentially with the increasing of lattice index. Under this parameter mechanism, the amplitude ψ_{b_n} of the left edge state at b-type site when $n \in [\frac{N}{2}+1, N]$ now becomes

$$\begin{aligned}
\psi_{b_{\frac{N}{2}+1}} &= \frac{-i\gamma}{J_1}\left(-\frac{J_1}{J_2}\right)^{N/2}\psi_{a_1}, \\
J_2\psi_{b_n} + J_1\psi_{b_{n+1}} &= -2i\gamma\left(-\frac{J_1}{J_2}\right)^{N/2}\psi_{a_1}, \\
\psi_{b_N} &= \frac{-2i\gamma}{J_2}\left(-\frac{J_1}{J_2}\right)^{N}\psi_{a_1}. \qquad \text{(A5)}
\end{aligned}$$

For the condition of thermodynamic limit ($N \sim \infty$), $\psi_{b_{\frac{N}{2}+1}} = \psi_{b_N} = 0$ can be obtained, which further leads $\psi_{b_n} = 0$ for $n \in [\frac{N}{2}+1, N]$. The above results clearly reveal that

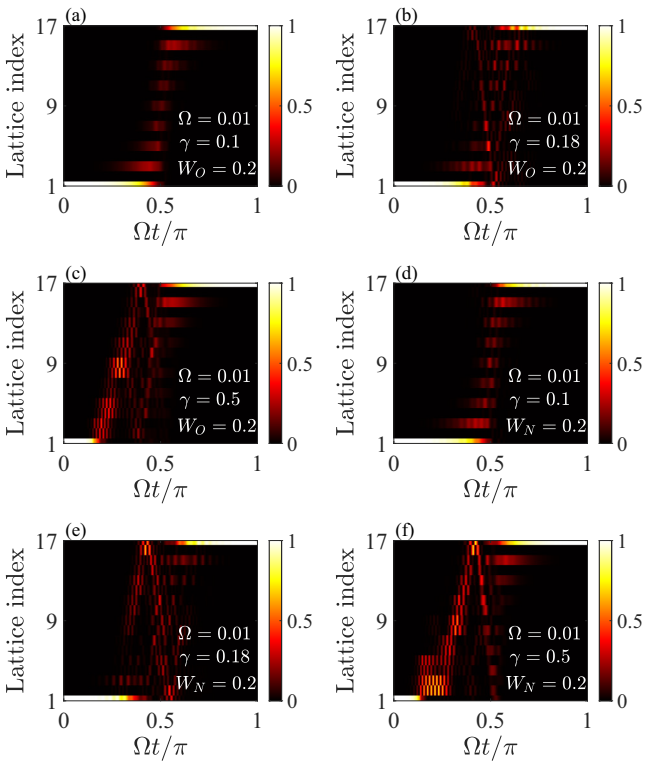

FIG. 9. The process of excitation transmission when disorder is added into the system. (a)–(c) When onsite disorder amplitude and varying rate satisfy $W_O = 0.2$ and $\Omega = 0.01$, the process of excitation transmission for $\gamma = 0.1$, $\gamma = 0.18$, and $\gamma = 0.5$. (d)–(f) When disorder amplitude in NN hopping and varying rate satisfy $W_N = 0.2$ and $\Omega = 0.01$, the process of excitation transmission for $\gamma = 0.1$, $\gamma = 0.18$, and $\gamma = 0.5$. In both cases, the random processes are taken 100 times. $J = 1$ is chosen as the energy unit.

the left edge state only occupies odd sites in the exponential way, i.e., the left edge state can be written as $|\Psi_{g,L}\rangle = |1,\ 0,\ \eta_L,\ 0, \ldots,\ \eta_L^{N-1},\ 0,\ \eta_L^N\rangle$ with localized index $\eta_L = -J_1/J_2$. Similarly, we can also obtain the right edge state via setting $E_{g,R} = i\gamma$, i.e., $|\Psi_{g,R}\rangle = |\eta_R^N,\ 0,\ \eta_R^{N-1},\ 0, \ldots,\ \eta_R,\ 0,\ 1\rangle$ with localized index $\eta_R = -J_2/J_1$. Actually, the form of the left edge state $|\Psi_{g,L}\rangle$ is essentially equivalent to $|\Psi_{g,R}\rangle$ since localized indices satisfy $|\eta_L| = 1/|\eta_R| = |J_1/J_2|$. For example, when $J_1 < J_2$ ($J_1 > J_2$) $|\Psi_{g,L}\rangle$ and $|\Psi_{g,R}\rangle$ are both localized at left (right) edge after normalization, implying that we can represent the gap state $|\Psi_g\rangle$ just via $|\Psi_{g,L}\rangle$ or $|\Psi_{g,R}\rangle$.

2. Average fidelity and robustness

As discussed in Sec. II A, the introduction of non-Hermitian parameter γ generates the windows of gapless points, which may lead the excitation to enter into bulk around the gapless point in the evolution process. Thus, the effects of gapless points for the excitation transmission should be investigated. In Sec. II B, we have discussed the controllable excitation transmission via defining the fidelity $F = |\langle R|\Psi_f\rangle|$. Actually, this definition of fidelity focuses on the success probability of excitation transferred to right edge without considering the intermediate process of evolved state.

Usually, if we are only interested in the case that excitation can be transferred to the right edge, this definition of fidelity is adequate to estimate the transmission efficiency. However, if we further consider the intermediate process of evolved state, this definition of fidelity should be modified. If we set the evolved state at any time as $\Psi(t)$, the fidelity at time t between $\Psi(t)$ and gap state $\Psi_g(t)$ (by replacing θ as Ωt) can be defined as $F_t = |\langle\Psi_g(t)|\Psi(t)\rangle|$. Thus, the average fidelity in the whole evolution process can be written as $\bar{F} = 1/T \sum_{t=0}^{t=\pi/\Omega} F_t$. Here T represents the length of time t for the numerical calculation. In this way, if the excitation initially prepared at the left edge evolving along the gap state strictly, the average fidelity satisfies $\bar{F} \sim 1$. Conversely, if the excitation entering into the bulk (generating diffusion) in the middle process of evolution, the average fidelity $\bar{F}$ will be decreased.

The average fidelity $\bar{F}$ versus γ and varying rate Ω is plotted in Fig. 8(a), in which the region of $\bar{F} \sim 1$ becomes much smaller compared with original definition of fidelity F [see Fig. 3(a)]. More specifically, when the parameters are within the region of $\bar{F} \sim 1$, the initial state will evolve along the gap state $|\Psi_g\rangle$, meaning the perfect excitation transmission. For example, when parameters satisfy $\Omega = 0.01$ and $\gamma = 0.1$, the perfect excitation transmission from the left edge to right edge can be implemented, as shown in Fig. 8(b). If we fix Ω and increase γ now, the excitation can still be transferred to the right edge but the intermediate process cannot evolve along the gap state, as shown in Figs. 8(c) and 8(d).

We stress that the perfect and imperfect excitation transmissions from the left edge to right edge are both robust to the disorder added into the system. For the given parameters shown in Figs. 8(b)–8(d), the excitation can still be transferred to the right edge successfully when the system has disorders added in onsite imaginary energy or NN hopping, as shown in Fig. 9. Especially, compared with the NN disorder, the evolution process of excitation transmission is much more robust to the onsite disorder. For example, when the system has mild onsite disorder with $W_O = 0.2$, the transmission process of excitation almost has no changes compared with the clean system, as shown in Figs. 9(a)–9(c). However, when the disorder is added into the NN hopping, the transmission from the left edge to right edge can still be implemented but the transmission process produces slight changes, as shown in Figs. 9(d)–9(f). This phenomenon means that the process of excitation transmission is much more robust to the onsite disorder compared with the disorder added into NN hopping, which differs from the results obtained in Figs. 3(e) and 3(f).

[1] M. Saffman, T. G. Walker, and K. Mølmer, Quantum information with rydberg atoms, Rev. Mod. Phys. **82**, 2313 (2010).

[2] D. Suter and G. A. Álvarez, Colloquium: Protecting quantum information against environmental noise, Rev. Mod. Phys. **88**, 041001 (2016).

[3] A. Galindo and M. A. Martín-Delgado, Information and computation: Classical and quantum aspects, Rev. Mod. Phys. **74**, 347 (2002).

[4] L. M. Duan and C. Monroe, Colloquium: Quantum networks with trapped ions, Rev. Mod. Phys. **82**, 1209 (2010).

[5] M. Z. Hasan and C. L. Kane, Colloquium: Topological insulators, Rev. Mod. Phys. **82**, 3045 (2010).

[6] X. L. Qi and S. C. Zhang, Topological insulators and superconductors, Rev. Mod. Phys. **83**, 1057 (2011).

[7] C. K. Chiu, J. C. Y. Teo, A. P. Schnyder, and S. Ryu, Classification of topological quantum matter with symmetries, Rev. Mod. Phys. **88**, 035005 (2016).

[8] A. Bansil, H. Lin, and T. Das, Colloquium: Topological band theory, Rev. Mod. Phys. **88**, 021004 (2016).

[9] C. Nayak, S. H. Simon, A. Stern, M. Freedman, and S. Das Sarma, Non-abelian anyons and topological quantum computation, Rev. Mod. Phys. **80**, 1083 (2008).

[10] J. Alicea, Y. Oreg, G. Refael, F. Von Oppen, and M. Fisher, Non-abelian statistics and topological quantum information processing in 1D wire networks, Nat. Phys. **7**, 412 (2011).

[11] G. Tkachov, P. Burset, B. Trauzettel, and E. M. Hankiewicz, Quantum interference of edge supercurrents in a two-dimensional topological insulator, Phys. Rev. B **92**, 045408 (2015).

[12] M. Bello, C. E. Creffield, and G. Platero, Long-range doublon transfer in a dimer chain induced by topology and ac fields, Sci. Rep. **6**, 1 (2016).

[13] C. Dlaska, B. Vermersch, and P. Zoller, Robust quantum state transfer via topologically protected edge channels in dipolar arrays, Quantum Sci. Technol. **2**, 015001 (2017).

[14] N. Lang and H. P. Büchler, Topological networks for quantum communication between distant qubits, npj Quantum Inf. **3**, 47 (2017).

[15] J. L. Tambasco, G. Corrielli, R. J. Chapman, A. Crespi, O. Zilberberg, R. Osellame, and A. Peruzzo, Quantum interference of topological states of light, Sci. Adv. **4**, eaat3187 (2018).

[16] N. Hao, P. Zhang, Z. Wang, W. Zhang, and Y. Wang, Topological edge states and quantum hall effect in the haldane model, Phys. Rev. B **78**, 075438 (2008).

[17] R. S. K. Mong and V. Shivamoggi, Edge states and the bulk-boundary correspondence in dirac Hamiltonians, Phys. Rev. B **83**, 125109 (2011).

[18] F. Zhang, C. L. Kane, and E. J. Mele, Surface states of topological insulators, Phys. Rev. B **86**, 081303(R) (2012).

[19] P. Roushan, J. Seo, C. V. Parker, Y. S. Hor, D. Hsieh, D. Qian, A. Richardella, M. Z. Hasan, R. J. Cava, and A. Yazdani, Topological surface states protected from backscattering by chiral spin texture, Nature (London) **460**, 1106 (2009).

[20] L. A. Wray, S. Y. Xu, Y. Xia, D. Hsieh, A. V. Fedorov, Y. S. Hor, R. J. Cava, A. Bansil, H. Lin, and M. Z. Hasan, A topological insulator surface under strong coulomb, magnetic and disorder perturbations, Nat. Phys. **7**, 32 (2011).

[21] T. Kitagawa, M. A. Broome, A. Fedrizzi, M. S. Rudner, E. Berg, I. Kassal, A. Aspuru-Guzik, E. Demler, and A. G. White, Observation of topologically protected bound states in photonic quantum walks, Nat. Commun. **3**, 882 (2012).

[22] S. Matsuura, P. Y. Chang, A. P. Schnyder, and S. Ryu, Protected boundary states in gapless topological phases, New J. Phys. **15**, 065001 (2013).

[23] Q. Wu, L. Du, and V. E. Sacksteder, Robust topological insulator conduction under strong boundary disorder, Phys. Rev. B **88**, 045429 (2013).

[24] M. Malki and G. S. Uhrig, Tunable edge states and their robustness towards disorder, Phys. Rev. B **95**, 235118 (2017).

[25] C. Chen, X. Ding, J. Qin, Y. He, Y. H. Luo, M.-C. Chen, C. Liu, X. L. Wang, W. J. Zhang, H. Li, L. X. You, Z. Wang, D. W. Wang, B. C. Sanders, C. Y. Lu, and J. W. Pan, Observation of Topologically Protected Edge States in a Photonic Two-Dimensional Quantum Walk, Phys. Rev. Lett. **121**, 100502 (2018).

[26] S. Hu, Y. Ke, and C. Lee, Topological quantum transport and spatial entanglement distribution via a disordered bulk channel, Phys. Rev. A **101**, 052323 (2020).

[27] D. G. Rothe and E. M. Hankiewicz, Tunable polarization in a beam splitter based on two-dimensional topological insulators, Phys. Rev. B **89**, 035418 (2014).

[28] X. S. Wang, Y. Su, and X. R. Wang, Topologically protected unidirectional edge spin waves and beam splitter, Phys. Rev. B **95**, 014435 (2017).

[29] M. Makwana, R. Craster, and S. Guenneau, Topological beam-splitting in photonic crystals, Opt. Express **27**, 16088 (2019).

[30] L. He, H. Y. Ji, Y. J. Wang, and X. D. Zhang, Topologically protected beam splitters and logic gates based on two-dimensional silicon photonic crystal slabs, Opt. Express **28**, 34015 (2020).

[31] W. P. Su, J. R. Schrieffer, and A. J. Heeger, Solitons in Polyacetylene, Phys. Rev. Lett. **42**, 1698 (1979).

[32] M. P. Estarellas, I. D'Amico, and T. P. Spiller, Topologically protected localised states in spin chains, Sci. Rep. **7**, 42904 (2017).

[33] F. Mei, G. Chen, L. Tian, S. L. Zhu, and S. Jia, Robust quantum state transfer via topological edge states in superconducting qubit chains, Phys. Rev. A **98**, 012331 (2018).

[34] M. I. N. Rosa, R. K. Pal, J. R. F. Arruda, and M. Ruzzene, Edge States and Topological Pumping in Spatially Modulated Elastic Lattices, Phys. Rev. Lett. **123**, 034301 (2019).

[35] S. Longhi, G. L. Giorgi, and R. Zambrini, Landau–zener topological quantum state transfer, Adv. Quantum Technol. **2**, 1800090 (2019).

[36] S. Longhi, Topological pumping of edge states via adiabatic passage, Phys. Rev. B **99**, 155150 (2019).

[37] L. Qi, G. L. Wang, S. Liu, S. Zhang, and H. F. Wang, Controllable photonic and phononic topological state transfers in a small optomechanical lattice, Opt. Lett. **45**, 2018 (2020).

[38] F. M. D'Angelis, F. A. Pinheiro, D. Guéry-Odelin, S. Longhi, and F. M. C. Impens, Fast and robust quantum state transfer in a topological Su-Schrieffer-Heeger chain with next-to-nearest-neighbor interactions, Phys. Rev. Res. **2**, 033475 (2020).

[39] N. E. Palaiodimopoulos, I. Brouzos, F. K. Diakonos, and G. Theocharis, Fast and robust quantum state transfer via a topological chain, Phys. Rev. A **103**, 052409 (2021).

[40] Y. E. Kraus, Y. Lahini, Z. Ringel, M. Verbin, and O. Zilberberg, Topological States and Adiabatic Pumping in Quasicrystals, Phys. Rev. Lett. **109**, 106402 (2012).

[41] F. Mei, S. L. Zhu, Z. M. Zhang, C. H. Oh, and N. Goldman, Simulating Z_2 topological insulators with cold atoms in a one-dimensional optical lattice, Phys. Rev. A **85**, 013638 (2012).

[42] M. Verbin, O. Zilberberg, Y. Lahini, Y. E. Kraus, and Y. Silberberg, Topological pumping over a photonic fibonacci quasicrystal, Phys. Rev. B **91**, 064201 (2015).

[43] F. Mei, J. B. You, W. Nie, R. Fazio, S.-L. Zhu, and L. C. Kwek, Simulation and detection of photonic chern insulators in a one-dimensional circuit-qed lattice, Phys. Rev. A **92**, 041805(R) (2015).

[44] F. Mei, Z. Y. Xue, D. W. Zhang, L. Tian, C. Lee, and S. L. Zhu, Witnessing topological weyl semimetal phase in a minimal circuit-qed lattice, Quantum Sci. Technol. **1**, 015006 (2016).

[45] E. Lustig, S. Weimann, Y. Plotnik, Y. Lumer, M. A. Bandres, A. Szameit, and M. Segev, Photonic topological insulator in synthetic dimensions, Nature (London) **567**, 356 (2019).

[46] E. Lustig and M. Segev, Topological photonics in synthetic dimensions, Adv. Opt. Photonics **13**, 426 (2021).

[47] C. F. Li, X. P. Li, and L. C. Wang, Topological phases of modulated su-schrieffer-heeger chains with long-range interactions, Europhys. Lett. **124**, 37003 (2018).

[48] X. L. Lü and H. Xie, Topological phases and pumps in the Su–Schrieffer–Heeger model periodically modulated in time, J. Phys.: Condens. Matter **31**, 495401 (2019).

[49] Y. X. Shen, L. S. Zeng, Z. G. Geng, D. G. Zhao, Y. G. Peng, and X. F. Zhu, Acoustic Adiabatic Propagation Based on Topological Pumping in a Coupled Multicavity Chain Lattice, Phys. Rev. Appl. **14**, 014043 (2020).

[50] L. S. Zeng, Y. X. Shen, Y. G. Peng, D. G. Zhao, and X. F. Zhu, Selective Topological Pumping for Robust, Efficient, and Asymmetric Sound Energy Transfer in a Dynamically Coupled Cavity Chain, Phys. Rev. Appl. **15**, 064018 (2021).

[51] L. Qi, G. L. Wang, S. Liu, S. Zhang, and H. F. Wang, Engineering the topological state transfer and topological beam splitter in an even-sized Su-Schrieffer-Heeger chain, Phys. Rev. A **102**, 022404 (2020).

[52] L. Qi, Y. Xing, X. D. Zhao, S. Liu, S. Zhang, S. Hu, and H. F. Wang, Topological beam splitter via defect-induced edge channel in the rice-mele model, Phys. Rev. B **103**, 085129 (2021).

[53] L. Qi, Y. Yan, Y. Xing, X. D. Zhao, S. Liu, W. X. Cui, X. Han, S. Zhang, and H. F. Wang, Topological router induced via long-range hopping in a Su-Schrieffer-Heeger chain, Phys. Rev. Res. **3**, 023037 (2021).

[54] J. Claes and T. L. Hughes, Skin effect and winding number in disordered non-Hermitian systems, Phys. Rev. B **103**, L140201 (2021).

[55] R. Sarkar, S. S. Hegde, and A. Narayan, Interplay of disorder and point-gap topology: Chiral modes, localization, and non-Hermitian Anderson skin effect in one dimension, Phys. Rev. B **106**, 014207 (2022).

[56] A. Szameit, Y. V. Kartashov, F. Dreisow, M. Heinrich, T. Pertsch, S. Nolte, A. Tünnermann, V. A. Vysloukh, F. Lederer, and L. Torner, Inhibition of Light Tunneling in Waveguide Arrays, Phys. Rev. Lett. **102**, 153901 (2009).

[57] I. L. Garanovich, S. Longhi, A. A. Sukhorukov, and Y. S. Kivshar, Light propagation and localization in modulated photonic lattices and waveguides, Phys. Rep. **518**, 1 (2012).

[58] L. Lu, J. D. Joannopoulos, and M. Soljačić, Topological photonics, Nat. Photonics **8**, 821 (2014).

[59] Y. Ke, X. Qin, F. Mei, H. Zhong, Y. S. Kivshar, and C. Lee, Topological phase transitions and thouless pumping of light in photonic waveguide arrays, Laser Photon. Rev. **10**, 995 (2016).

[60] T. Ozawa, H. M. Price, A. Amo, N. Goldman, M. Hafezi, L. Lu, M. C. Rechtsman, D. Schuster, J. Simon, O. Zilberberg, and I. Carusotto, Topological photonics, Rev. Mod. Phys. **91**, 015006 (2019).

[61] Q. Cheng, Y. Pan, H. Wang, C. Zhang, D. Yu, A. Gover, H. Zhang, T. Li, L. Zhou, and S. Zhu, Observation of Anomalous π Modes in Photonic Floquet Engineering, Phys. Rev. Lett. **122**, 173901 (2019).

[62] M. Kulishov, J. M. Laniel, N. Bélanger, and D. V. Plant, Trapping light in a ring resonator using a grating-assisted coupler with asymmetric transmission, Opt. Express **13**, 3567 (2005).

[63] M. Greenberg and M. Orenstein, Unidirectional complex gratings assisted couplers, Opt. Express **12**, 4013 (2004).

[64] J. Čtyroký, V. Kuzmiak, and S. Eyderman, Waveguide structures with antisymmetric gain/loss profile, Opt. Express **18**, 21585 (2010).

[65] J. Mu, M. Dijkstra, J. Korterik, H. Offerhaus, and S. M. García-Blanco, High-gain waveguide amplifiers in Si_3N_4 technology via double-layer monolithic integration, Photon. Res. **8**, 1634 (2020).

[66] E. Awad, A novel metamaterial gain-waveguide nanolaser, Opt. Laser Technol. **142**, 107202 (2021).